TID-4500, UC-51
Geology and Mineralogy

Lawrence Radiation Laboratory
UNIVERSITY OF CALIFORNIA
LIVERMORE

UCRL-50963

HIGH-PRESSURE MECHANICAL PROPERTIES OF ROCKS FROM WAGON WHEEL NO. 1, PINEDALE, WYOMING

R. N. Schock
H. C. Heard
D. R. Stephens

Contents

HIGH-PRESSURE MECHANICAL PROPERTIES OF ROCKS FROM WAGON WHEEL NO. 1, PINEDALE, WYOMING

Abstract

The strength, volume, acoustic velocities, and relationships between shear stress and shear strain were studied as functions of pressure for selected sedimentary rocks in the interval 8942 ft - 10,518 ft from Wagon Wheel No. 1. Typical moduli for undeformed sandstone at overburden pressure (~750 bar) are μ = 0.200 Mb, K = 0.210 Mb, and ν = 0.13. With increasing shear stress μ decreases and ν increases, indicating inelastic deformation. The sandstones show almost no purely elastic deformation under shear stress due presumably to the low strength of the fine-grained detrital matrix. At laboratory strain rates (~10^{-5} sec^{-1}) when loading along a path thought to simulate the shock-wave trajectory, the failure surface is not intersected either upon loading or on any extreme unloading path. Higher strain rates may favor intersection, although we have no compelling evidence.

Symbols and Units

- σ - stress denoted by subscript as maximum principle (1), intermediate and minimum principal stress or confining pressure (2,3)
- ϵ - strain denoted by subscript as radial (r), longitudinal (ℓ), or volume (V)
- C_{ij} - elastic constant σ_i/ϵ (Mbar)
- β - isothermal volume compressibility = $-\frac{1}{V}\frac{dV}{dP}$ ($Mbar^{-1}$)
- K - bulk modulus = $1/\beta$ (Mbar)
- μ - shear modulus (Mbar)
- E - Young's modulus (Mbar)
- ν - Poisson's ratio
- ρ - density (g cm^{-3})
- V_P, V_S - compressional and shear velocity (km sec^{-1})
- τ - shear strength $(\sigma_1 - \sigma_3)/2$ (kbar)
- P_m - $(\sigma_1 + 2\sigma_3)/3$ (kbar)
- bar - 10^6 dyne cm^{-2} = 10^{-3} kbar = 10^{-6} Mbar

Introduction

Project Wagon Wheel is designed to utilize nuclear explosives to stimulate gas flow by fracturing or otherwise altering the existing reservoir to increase rock permeability. The site is El Paso Natural Gas Company's Wagon Wheel No. 1 well, NW 1/4 Section 5, T30N, R108W, Sublette County, Wyoming. The main purpose of our equation of state (EOS) measurements is to provide input

to calculational codes in order to predict the effects of large explosions on the surrounding media. Primary among these effects is the extent and degree of fracturing produced.

The rocks studied here are from the depth interval between 8942 ft and 10,518 ft. This interval represents the upper formations (Lewis and Lance) of the Cretaceous Mesa Verde group and the lower part of the Paleocene Fort Union formation. They are for the most part massive sandstones with thin shale and siltstone interbeds and with few fractures. The sandstones tend to be fine- to very fine-grained and moderately sorted graywackes. They are in general notable for their low feldspar content[1] and would be classified as subgraywackes in the scheme of Pettijohn[2] or as low-rank graywackes by Krynine.[3]

Our EOS measurements include: The failure surface to 13 kbar mean pressure; the pressure-volume (P-V) curve on loading to, and subsequent unloading from, 40 kbar; acoustic compressional and shear velocities as functions of confining pressure to 10 kbar; and three-dimensional strain measurements along various loading and unloading paths below the failure surface up to ~5 kbar mean pressure. Tests on the Wagon Wheel rocks were made in both the dry and the 50%-saturated states, the latter to approximate the in-situ water content as determined by well-log and core analysis.[4]

Experimental

The samples selected for the studies described in this report are recorded in Table 1 along with their depths, densities as determined in the laboratory, water content released on heating to 110°C, and log descriptions.[‡] The experimental techniques used for the EOS measurements have been described previously.[5-9] Briefly, triaxial strength is determined from one-dimensional stress-axial strain measurements on jacketed cylindrical samples compressed to failure at various fluid pressures. P-V data are obtained in a piston-cylinder device where the advance of the piston with increasing load is monitored with high precision. Acoustic velocities are obtained by sending a 1 MHz wave through jacketed samples and measuring the corresponding travel time. Precise three-dimensional strain measurements are accomplished with foil-strain gages cemented to either (A) an epoxy coated rock sample, or (B) a metal jacketed sample, depending on the stress levels desired. For end loads below about 4 kbar, a fluid loading system and (A), above, are used; above this pressure samples are jacketed as in (B), above, and a solid piston furnishes axial loads. These strain experiments yield, in addition to the failure envelope, elastic and inelastic deformation moduli over a range of stress states below the failure envelope. These moduli include the compressibility, shear modulus, and Poisson's ratio, both on loading and on unloading.

‡El Paso Natural Gas Co., lithologic log.

Table 1. Summary of Wagon Wheel rocks used in EOS measurements.

Depth (ft)	Log description[a]	Zero pressure density (g cm^{-3})	Percent H_2O
8944.6- 8945.5	very fine-grained sandstone	2.51	1.2
8998.2- 8999.5	siltstone	2.60	0.8
10178.6-10179.7	medium-grained sandstone	2.40	1.6
10236.5-10237.8	fine-grained sandstone	2.45	1.0
11060.1-11061.6	medium-grained sandstone	2.43	—

[a]El Paso Natural Gas Co., lithologic log.

DETERMINATION OF THE FAILURE ENVELOPE

Only one type of sandstone was evaluated for strength properties. This was the relatively fine-grained material from a depth of 10,237 ft. In addition to the triaxial compression tests at confining pressures ranging up to 7 kbar, uniaxial compression and Brazil tests were performed on dry material at atmospheric pressure. All experiments were carried out at strain rates near 10^{-4} sec^{-1}. Several tests were performed on the partially- and fully-saturated sandstone to evaluate the effects of fluid saturation on strength and ductility. Data were taken in the form of force-displacement curves. After recalculation to differential stress-strain curves, the ultimate strength (in those tests which exhibited brittle behavior) or differential stress taken at 5% strain (for those experiments which were macroscopically ductile) were noted. The values of the principal stresses at failure for each test are summarized in Table 2.

Brittle behavior may be characterized by a sudden change of slope of the stress-strain curve at the yield point followed either by a complete loss of cohesion in the test sample with a subsequent drop in differential stress to zero, or by continued fracturing and rehealing of the rock, characterized by sharp downward breaks in the slope of the curve. Fracture is often accompanied by an audible report. Ductile behavior is taken to be the absence of any sharp downward breaks in slope after the yield point, with the sample achieving at least 5% strain before fracture. On the scale of the test sample, ductile behavior may be accomplished by homogeneously distributed fracture and rotation of small elements of material, or by plastic flow (twinning or translation) on any scale. In the case of the sandstone we are considering, overall ductile behavior is due predominantly to the former mechanism with the individual brittle quartz grains taking up the local displacements.

Figure 1 illustrates the shear stress-mean pressure failure envelope for dry rock based upon the principal stress data from Table 2. The approximate transition from macroscopic brittle fracture to ductile flow is noted to occur on this curve at about 6 kbar mean pressure. Below this region, extensile and shear fractures predominate, but complete loss of cohesion of the sandstone occurs only below

Table 2. Summary of failure test data, Wagon Wheel No. 1, 10237-ft samples.

Test type	σ_1 (kbar)	σ_2 (kbar)	σ_3 (kbar)	Behavior	τ (kbar)	P_m (kbar)
Brazil	0.33	0	-0.11	Brittle	0.22	0.07
Brazil	0.33	0	-0.11	Brittle	0.22	0.07
Triaxial	1.41	0	0	Brittle	0.70	0.47
Triaxial	1.64	0	0	Brittle	0.82	0.55
Triaxial	1.60	0	0	Brittle	0.80	0.53
Triaxial	6.33	1.00	1.00	Brittle	2.65	2.78
Triaxial	9.35	2.00	2.00	Brittle	3.68	4.45
Triaxial	12.58	3.00	3.00	Transitional	4.79	6.19
Triaxial	11.92	3.00	3.00	Transitional	4.46	5.97
Triaxial[a]	11.30	3.00	3.00	Transitional	4.15	5.77
Triaxial[b]	6.14	3.00	3.00	Brittle	1.57	4.05
Triaxial	15.87	4.00	4.00	Ductile	5.94	7.96
Triaxial	19.55	5.00	5.00	Ductile	7.28	9.85
Triaxial	18.84	5.00	5.00	Ductile	6.92	9.61
Triaxial	23.35	6.00	6.00	Ductile	8.68	11.78
Triaxial	25.84	7.00	7.00	Ductile	9.42	13.28
Triaxial[a]	26.20	7.00	7.00	Ductile	9.60	13.40

[a]50% of pore volume filled with water.

[b]Pore volume fully saturated with water.

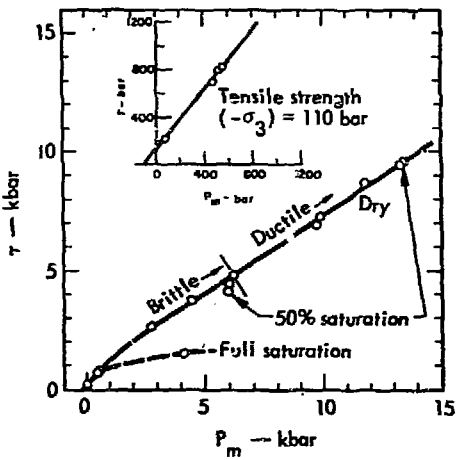

Fig. 1. 10,237 ft: Failure envelope.

~1 kbar. Between these mean pressures cohesion is retained, at least up to average strains of ~10-15%. Above this brittle-ductile transition, little fracture or faulting is present (on the scale of the sample); the stress-strain curve shows work hardening and the strains are more or less homogeneously distributed throughout the sample (at least in the scale of tens of microns). Inspection of Fig. 1 shows the envelope to be nearly linear, except at low pressures, with a slope of about 0.67. There is no indication of a decrease in slope, even at the highest pressure; the mean pressure where this material approaches a von Mieses solid is unknown.

The limiting shear strength is probably in the 20-25 kbar range. The lower portion (non-linear region) is shown at an expanded scale in the top insert. The tensile strength, as determined from Brazil tests, seems to be moderately high (~110 bars) and very reproducible.

In addition to the dry data discussed above, several tests were run at 3-7 kbar confining pressure at 50% saturation; others were run on rocks in the fully saturated state. Comparison of all data in Fig. 1 shows that the fully saturated sandstone is very much weaker and more brittle than its dry counterpart; in fact the wet shear strength is only about 1/3 of the dry value (Table 2). This behavior is to be expected for this type of rock and is well documented in the literature.[8] The several samples tested in the 50%-saturated state behaved very nearly the same as the dry sandstone (Fig. 1, Table 2). This occurs because at confining pressures ranging to 7 kbar, the solid matrix framework does not fully collapse to eliminate the initial 50%-gas-filled porosity. For this degree of saturation and a porosity of 8%, collapse would be expected at approximately 30 kbar mean pressure. At this point, the level of the failure envelope should decay to some lower value.

HYDROSTATIC PRESSURE-VOLUME CHARACTERISTICS

The pressure-volume (P-V) hydrostats for Wagon Wheel sandstone have been determined for rock from the 8945-ft and 10,237-ft levels. Compressibility data for the 8945 ft material are shown in Fig. 2; P-V data integrated from the compressibilities and the initial density of 2.512 g/cm^3 are shown in Fig. 3 and Table 3. These data are on 50%-saturated rock containing 1.2% H_2O. At overburden pressure for the Wagon Wheel rocks (about 750 bar) the compressibility is 4.9 Mbar^{-1}, in good agreement with well logs* and with compressibilities determined from principal strain measurements. The sandstone is

*Birdwell velocity log.

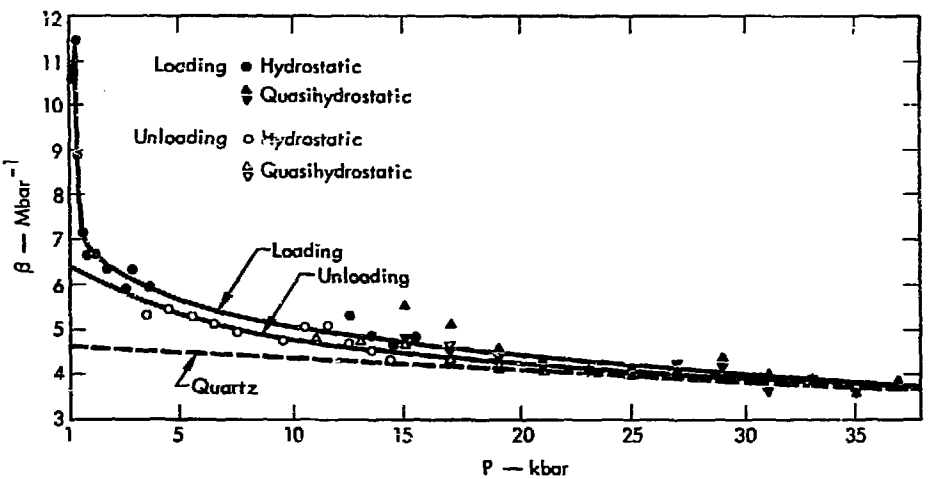

Fig. 2. 8945 ft: Compressibility versus pressure.

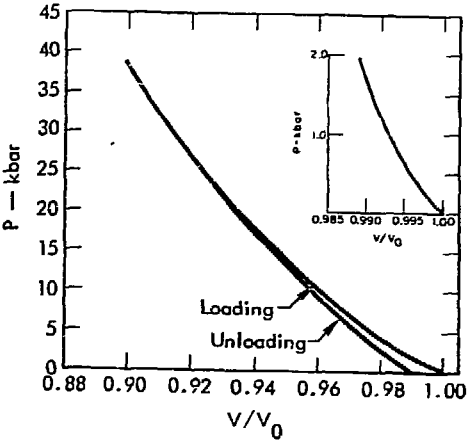

Fig. 3. 8945 ft: Pressure versus V/V_0.

about 10% compressible to 39 kbar and exhibits ~1% irreversible compaction on unloading.

The data in Fig. 2 were taken with several samples and reasonable agreement is noted. The hydrostatic volume compressibilities are computed as $\beta_{vol} = 3\,\beta_{\ell}$ where β_{ℓ} is the linear compressibility in the direction normal to the bedding. If the rock is not entirely isotropic, there will be some error in the volume compressibilities.

Reliable compressibilities were not obtained upon unloading below 3 kbar and thus the data shown in Fig. 1 involve a short

Table 3. Pressure vs V/V_0 for Wagon Wheel sandstone, 8945 ft. $\rho_0 = 2.512\ g/cm^3$. 50% saturated, 1.2 wt-% water.

	V/V_0			$v\ (cm^3/g)$		
(kbar)	Loading	Unloading from 1 kbar	Unloading from 39 kbar	Loading	Unloading from 1 kbar	Unloading from 39 kbar
0	1.000	0.99972	0.99947	0.39809	0.39798	0.39430
0.05	0.99958					
0.1	0.99916					
0.15	0.99860					
0.25	0.99750					
0.5	0.99575					
0.75						
1	0.99319		0.98615	0.39548		0.39259
2	0.98672			0.39360		
3	0.98458		0.97848	0.39195		0.38952
4	0.98068			0.39040		
5	0.97762		0.97162	0.38894		0.38679
6	0.97352			0.38755		
7	0.97018		0.96543	0.38622		0.38433
9	0.96383		0.95976	0.38369		0.38207
11	0.95790		0.95439	0.38143		0.37993
13	0.95225		0.94928	0.37908		0.37790
15	0.94687		0.94442	0.37694		0.37596
17	0.94177		0.93976	0.37491		0.37411
19	0.93690		0.93532	0.37297		0.37234
21	0.93228		0.93107	0.37113		0.37065
23	0.92786		0.92701	0.36937		0.36903
25	0.92366		0.92312	0.36770		0.36748
27	0.91964		0.91934	0.36610		0.36598
29	0.91580		0.91567	0.36457		0.36452
31	0.91213		0.91212	0.36311		0.36310
33	0.90864		0.90864	0.36172		0.36172
35	0.90530		0.90530	0.36039		0.36039
37	0.90211		0.90211	0.35912		0.35912
39	0.89909		0.89909	0.35792		0.35792

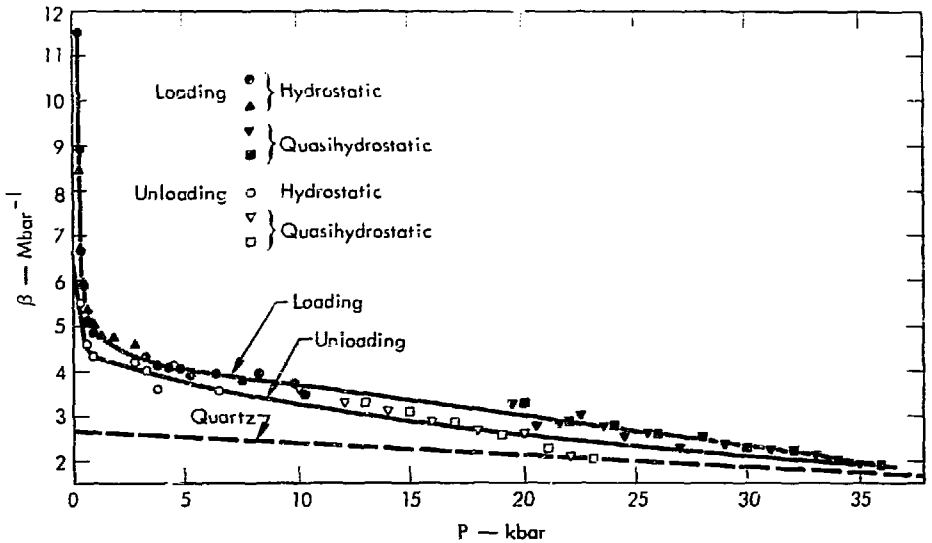

Fig. 4. 10,237 ft: Compressibility versus pressure.

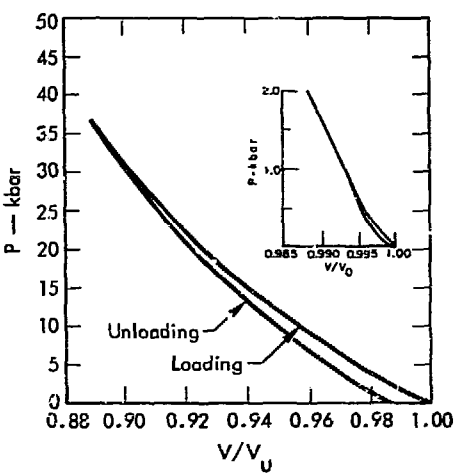

Fig. 5. 10,237 ft: Pressure versus V/V_0.

extrapolation to zero pressure. It should be mentioned that reliable data were not obtained with the quasihydrostatic apparatus below 10-15 kbar for any of the Wagon Wheel samples. These points are not shown in Fig. 2 or in Fig. 4 (see below).

Compressibility data for the 10,237-ft sandstone are shown in Fig. 4, and the integrated P-V data are given in Fig. 5 and in Table 4. This rock was also 50% saturated and contained 1.0% H_2O. At overburden pressure the compressibility is 5.0 $Mbar^{-1}$, slightly higher than for the 8945-ft sample but still in fair agreement with the logs and with our other strain measurements. This rock is 10-15% more compressible at high pressures than is the 8945-ft sample, in accordance with the lower initial density of the 10,237-ft sample (2.45 vs 2.48 g/cm^3). The inital porosity is higher and thus one would expect the rock to be more compressible. The irreversible compaction upon unloading from high pressure is 1.3% for the 10,236-ft sample, compared to 1% for the 8945-ft material, further supporting the higher initial porosity of the 10,237-ft samples.

Table 4. Pressure vs V/V0 for Wagon Wheel sandstone, 10237 ft. ρ_0 = 2.45 to 2.48 g/cm^3. 50% saturated. 1.0 wt-% water.

P (kbar)	V/V0 Loading	V/V0 Unloading from 1 kbar	V/V0 Unloading from 37 kbar
0	1.000	0.99940	0.98744
0.05	0.99938		
0.1	0.99877	0.99795	
0.15	0.99818		
0.25	0.99716	0.99661	
0.5	0.99547	0.99521	
0.75	0.99415	0.99412	
1	0.99292	0.99292	0.98219
1.5	0.99057		
2	0.98831		0.97803
3	0.98399		0.97403
4	0.97988		
5	0.97591		0.96649
6	0.97205		
7	0.96827		0.95947
9	0.96095		0.95288
11	0.95394		0.94668
13	0.94722		0.94081
15	0.94081		0.93524
17	0.93468		0.92995
19	0.92885		0.92491
21	0.92330		0.92012
23	0.91802		0.91555
25	0.91302		0.91121
27	0.90829		0.90707
29	0.90386		0.90309
31	0.89968		0.89926
33	0.89575		0.89559
35	0.89208		0.89205
37	0.88867		0.88867

At high pressures the porosity is expected to decrease due to inelastic failure of the rock around the open pore. One

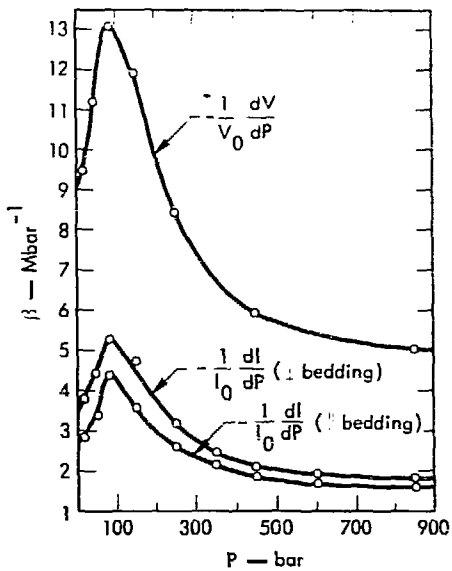

Fig. 6. 10,237 ft: Directional compressibility versus pressure below 900 bar.

then expects that the specific volumes of rocks with similar mineralogy but different porosities will approach one another. In fact the specific volumes of the two rocks would be identical at 35 kbar if an initial density of 2.475 were assumed for the 10,237-ft sandstone.

Figure 6 displays the compressibilities determined for 10,237-ft samples from measured principal strains to approximately 1 kbar. The different compressibilities in, and normal to, the bedding plane show, as is expected, that the rock is anisotropic in its deformation characteristics. The degree of anisotropy in hydrostatic compression is about 5% up to these pressures, however; independent evidence[6] suggests that at higher pressures it is even less. The curves all show a marked leveling-off of the sharp decrease

in compressibility at around 500 bar; this is believed to represent the return of the rock to overburden pressure, implying a certain amount of fracture-produced volume which was induced when the sample was recovered. The initial increase in compressibility is indicative of the progressive collapse of fractures and voids as their individual strengths are overcome.

LABORATORY ACOUSTIC VELOCITIES AND DERIVED ELASTIC MODULI TO 10 kbar

All samples were treated as being transversely anisotropic and the complete elastic constant matrix as a function of pressure was determined from acoustic velocity measurements for the siltstone (8999 ft) and for the two sandstones (10,237 ft and 11,060 ft). The axis of principal symmetry is taken normal to the plane of the bedding, and five independent velocities are measured to 10 kbar. The results for the 10,237-ft sandstone are shown in Table 5, where the principal axis is 3, minor axes are 1 and 2 in the isotropic plane, and a simplified suffix notation ($12 \rightarrow 6$, $13 \rightarrow 5$, $23 \rightarrow 4$, $33 \rightarrow 3$, $22 \rightarrow 2$, and $11 \rightarrow 1$) is used to simplify the ij and kℓ suffixes in the elasticity equation

$$\sigma_{ij} = C_{ijk\ell}\, \epsilon_{k\ell}.$$

Densities are determined by continuously integrating the computed bulk modulus. As expected the rock is stiffer (i.e., its elastic constant is higher) in the bedding plane (C_{11}, C_{66}) than across it (C_{33}, C_{44}) and this relationship holds to 10 kbar. However, there is a significant decrease in this anisotropy with pressure as reflected in the elastic constants reduced to individual moduli (E_{11}, E_{33}; β_{11}, β_{33}; ν_{12}, ν_{31}). The velocities determined in the laboratory at 800 bar (near overburden) are somewhat higher than the well log velocities*; i.e., compare $V_P = 4.89$ with $V_P = 4.65$ km sec^{-1} and $V_S = 2.97$ with $V_S = 2.32$ km sec^{-1}. This is not unexpected since the travel path in the laboratory is some 27.0 mm compared with 5.35 m in the well hole. Thus, large fractures and joints present in-situ (and not present in laboratory samples) would retard travel-times over those in the more homogeneous rock mass. In addition, imperfections induced by drilling

*Birdwell velocity log.

Table 5. Velocities and elastic constants to 10 kbar, Wagon Wheel No. 1, 10237 ft.

Pressure (kbar)	C_{11}	C_{66}	C_{33}	C_{44}	C_{13}	C_{12}	E_{11}	E_{33}	ν_{12}	ν_{13}	ν_{31}	ρ (gcm^3)	β_{11}	β_{33}	β_{vol}	V_{P11}	V_{S12}	V_{P33}	V_{S31}	$V_{P45°-3}$
0.00	0.428	0.155	0.379	0.148	0.106	0.118	0.379	0.338	0.221	0.217	0.194	2.440	1.461	1.813	4.775	4.189	2.523	3.941	2.465	4.067
0.10	0.478	0.171	0.414	0.156	0.101	0.136	0.427	0.380	0.245	0.184	0.164	2.441	1.338	1.766	4.441	4.427	2.649	4.116	2.534	4.203
0.20	0.519	0.187	0.457	0.171	0.051	0.146	0.468	0.432	0.255	0.149	0.137	2.442	1.274	1.680	4.228	4.609	2.764	4.325	2.643	4.344
0.30	0.556	0.204	0.500	0.185	0.102	0.149	0.505	0.471	0.239	0.155	0.145	2.443	1.201	1.510	3.911	4.772	2.889	4.525	2.753	4.528
0.40	0.581	0.214	0.528	0.201	0.119	0.154	0.525	0.489	0.229	0.174	0.163	2.444	1.137	1.380	3.653	4.875	2.956	4.648	2.867	4.693
0.60	0.599	0.220	0.563	0.208	0.147	0.159	0.535	0.506	0.215	0.204	0.193	2.446	1.085	1.212	3.382	4.950	3.000	4.796	2.913	4.834
0.80	0.612	0.224	0.585	0.216	0.143	0.164	0.548	0.532	0.224	0.190	0.184	2.448	1.069	1.187	3.325	5.002	3.025	4.887	2.972	4.897
1.00	0.622	0.227	0.596	0.220	0.148	0.169	0.556	0.541	0.225	0.193	0.187	2.449	1.048	1.157	3.252	5.040	3.042	4.933	2.996	4.943
1.50	0.640	0.231	0.616	0.225	0.148	0.179	0.571	0.562	0.237	0.183	0.180	2.453	1.016	1.137	3.170	5.108	3.067	5.009	3.031	4.999
2.00	0.655	0.234	0.624	0.228	0.155	0.187	0.580	0.567	0.242	0.188	0.184	2.457	0.983	1.114	3.079	5.162	3.084	5.041	3.048	5.045
3.00	0.672	0.238	0.642	0.232	0.169	0.196	0.591	0.576	0.241	0.200	0.195	2.465	0.946	1.059	2.951	5.221	3.108	5.103	3.070	5.116
4.00	0.682	0.241	0.655	0.235	0.179	0.201	0.597	0.583	0.240	0.208	0.203	2.472	0.925	1.020	2.871	5.254	3.120	5.149	3.084	5.162
6.00	0.701	0.245	0.682	0.239	0.188	0.213	0.611	0.605	0.248	0.207	0.205	2.486	0.892	0.976	2.760	5.316	3.139	5.237	3.099	5.221
8.00	0.721	0.247	0.702	0.241	0.202	0.227	0.619	0.615	0.255	0.215	0.214	2.500	0.856	0.931	2.643	5.369	3.141	5.298	3.108	5.282
10.00	0.730	0.248	0.722	0.244	0.223	0.233	0.620	0.619	0.248	0.232	0.232	2.513	0.848	0.867	2.543	5.388	3.144	5.361	3.118	5.344

would further add to this effect. Again as expected, the moduli derived from velocity measurements are higher than those measured directly; i.e., compare an acoustic β_{vol} = 3.325 $Mbar^{-1}$ at overburden with the value = 5.1 $Mbar^{-1}$ in Fig. 6. This is a well-known manifestation of cracks and fractures at low pressures, since the acoustic wave is insensitive to a finite percentage of these flaws which, as they close, are significant to the real moduli. Thus at higher pressures the two differently-determined values approach one another (Fig. 3 and Table 5).

Tables 6 and 7 illustrate similar results for the siltstone (8999 ft) and the sandstone (11,060 ft) and one may draw analogous conclusions. Table 8 shows the velocities determined normal to the bedding for the 10,179-ft sandstone sample and the moduli derived therefrom. Significantly, these data show that this material is similar in its elastic properties to the sandstones from other depths.

CONTROLLED STRESS-STRAIN LOADING PATHS

The stress-strain properties in nonhydrostatic loading were extensively examined for two rock-types, the sandstone from 10,237 ft and the siltstone at 8999 ft. In addition the sandstone from 10,179 ft received limited attention. Figures 7 and 8 show the results obtained in normal

Table 6. Velocities and elastic constants to 10 kbar, Wagon Wheel No. 1, 8999 ft.

Pressure (kbar)	C_{11}	C_{66}	C_{33}	C_{44}	C_{13}	C_{12}	E_{11}	E_{33}	ν_{12}	ν_{13}	ν_{31}	ρ (g cm^{-3})	β_{11}	β_{33}	β_{vol}	V_{P11}	V_{S12}	V_{P33}	V_{S31}	$V_{P45°-3}$
0.00	0.503	0.204	0.479	0.179	0.077	0.095	0.476	0.458	0.167	0.137	0.132	2.600	1.462	1.608	4.532	4.397	2.860	4.291	2.626	4.225
0.20	0.531	0.210	0.503	0.130	0.086	0.112	0.498	0.481	0.188	0.139	0.134	2.602	1.151	1.525	4.227	4.516	2.839	4.199	2.701	4.346
0.50	0.561	0.219	0.527	0.200	0.090	0.123	0.525	0.503	0.197	0.138	0.132	2.606	1.268	1.462	3.997	4.642	2.900	4.499	2.767	4.454
1.00	0.607	0.232	0.562	0.211	0.099	0.143	0.563	0.536	0.212	0.139	0.132	2.611	1.151	1.372	3.678	4.822	2.982	4.641	2.846	4.604
2.00	0.673	0.244	0.620	0.227	0.139	0.185	0.606	0.575	0.239	0.170	0.162	2.620	0.975	1.177	3.126	5.070	3.054	4.865	2.942	4.862
3.00	0.714	0.251	0.663	0.236	0.164	0.212	0.630	0.605	0.255	0.184	0.177	2.628	0.891	1.268	2.651	5.223	3.090	5.024	2.995	5.022
4.00	0.745	0.256	0.702	0.243	0.180	0.232	0.649	0.636	0.266	0.189	0.185	2.635	0.840	0.992	2.672	5.318	3.120	5.163	3.040	5.137
5.00	0.774	0.262	0.735	0.249	0.201	0.251	0.665	0.637	0.272	0.199	0.197	2.642	0.795	0.924	2.514	5.411	3.146	5.277	3.068	5.244
6.00	0.796	0.267	0.760	0.254	0.228	0.263	0.676	0.662	0.257	0.220	0.215	2.648	0.759	0.861	2.378	5.484	3.174	5.357	3.094	5.344
7.00	0.817	0.272	0.792	0.253	0.247	0.273	0.687	0.670	0.264	0.243	0.227	2.655	0.731	0.816	2.281	5.547	3.200	5.427	3.121	5.426
8.00	0.836	0.277	0.803	0.262	0.253	0.283	0.702	0.689	0.269	0.230	0.226	2.661	0.714	0.796	2.225	5.605	3.224	5.494	3.146	5.480
9.00	0.857	0.281	0.823	0.269	0.254	0.295	0.719	0.712	0.279	0.222	0.220	2.667	0.694	0.766	2.175	5.670	3.247	5.557	3.173	5.530
10.00	0.878	0.286	0.801	0.274	0.273	0.306	0.727	0.675	0.272	0.248	0.231	2.672	0.660	0.799	2.119	5.732	3.270	5.474	3.202	5.575

Table 7. Velocities and elastic constants to 10 kbar, Wagon Wheel No. 1, 11060 ft.

Pressure (kbar)	C_{11}	C_{66}	C_{33}	C_{44}	C_{13}	C_{12}	E_{11}	E_{33}	ν_{12}	ν_{13}	ν_{31}	ρ (g cm^{-3})	β_{11}	β_{33}	β_{vol}	V_{P11}	V_{S12}	V_{P33}	V_{S31}	$V_{P45°-3}$
0.00	0.429	0.159	0.400	0.110	0.098	0.111	0.386	0.364	0.214	0.193	0.182	2.430	1.537	1.746	4.829	4.200	2.559	4.058	2.568	4.141
0.10	0.472	0.169	0.421	0.166	0.092	0.135	423	0.393	0.254	0.164	0.152	2.431	1.377	1.772	4.525	4.408	2.634	4.161	2.614	4.236
0.20	0.5.2	0.179	0.455	0.179	0.078	0.154	0.459	0.437	0.282	0.123	0.117	2.432	1.297	1.734	4.347	4.588	2.712	4.326	2.713	4.351
0.40	0.535	0.194	0.532	0.146	0.123	0.166	0.489	0.486	0.258	0.179	0.178	2.434	1.152	1.326	3.629	4.774	2.529	4.673	2.941	4.675
0.60	0.575	0.204	0.559	0.205	0.132	0.163	0.510	0.513	0.251	0.176	0.177	2.436	1.124	1.259	3.506	4.855	2.892	4.792	2.901	4.770
0.80	0.586	0.208	0.576	0.209	0.136	0.171	0.520	0.528	0.250	0.176	[illegible]	2.438	1.104	1.216	3.424	4.901	2.919	4.862	2.926	4.824
1.00	0.594	[illegible]	0.588	0.212	0.142	0.171	0.526	0.539	0.242	0.191	0.185	2.439	1.087	1.176	3.350	4.945	2.939	4.912	2.946	4.868
2.00	0.612	0.217	0.617	0.214	0.170	0.177	0.535	0.544	0.240	0.212	0.215	2.447	1.041	1.046	[illegible]	4.995	2.950	5.022	[illegible]	4.996
3.00	0.629	0.221	0.630	0.223	0.194	0.186	0.541	0.517	0.222	0.240	0.219	2.455	0.954	0.974	2.962	[illegible]	3.003	5.065	3.011	5.085
4.00	0.642	0.224	0.640	[illegible]	0.215	[illegible]	0.544	0.513	[illegible]	[illegible]	0.237	2.462	[illegible]	[illegible]	[illegible]	5.103	[illegible]	5.100	3.030	5.152
5.00	0.653	0.227	0.650	0.223	0.231	0.200	0.547	0.524	[illegible]	[illegible]	0.271	[illegible]	[illegible]	0.874	2.741	5.145	[illegible]	[illegible]	3.039	5.205
6.00	0.664	0.230	[illegible]	0.230	[illegible]	0.205	[illegible]	0.550	[illegible]	[illegible]	[illegible]	[illegible]	[illegible]	[illegible]	2.675	5.180	3.045	5.146	3.047	5.243
7.00	0.674	0.232	[illegible]	0.242	0.255	0.210	[illegible]	0.514	[illegible]	[illegible]	[illegible]	[illegible]	[illegible]	[illegible]	2.607	5.212	3.057	[illegible]	3.054	5.282
8.00	0.665	0.235	[illegible]	[illegible]	0.257	[illegible]	0.561	0.532	[illegible]	[illegible]	[illegible]	[illegible]	0.577	0.921	2.576	5.245	073	[illegible]	3.039	5.300
9.00	[illegible]	0.238	[illegible]	0.234	0.254	[illegible]	0.573	0.515	0.295	[illegible]	0.277	[illegible]	[illegible]	[illegible]	[illegible]	[illegible]	087	5.206	3.062	5.306
10.00	0.700	0.241	0.632	0.245	0.247	[illegible]	[illegible]	[illegible]	0.212	0.266	[illegible]	2.502	[illegible]	0.641	[illegible]	[illegible]	3.102	5.222	3.063	5.302

Table 8. Velocities normal to bedding and derived elastic constants to 10 kbar, Wagon Wheel No. 1, 10179 ft.

Pressure (kbar)	ρ (g cm^{-3})	V_P	V_S	K	μ	ν	E
0.00	2.400	3.58	2.28	0.142	0.124	0.161	0.289
0.10	2.402	3.54	2.43	0.164	0.142	0.164	0.331
0.20	2.403	4.17	2.61	0.182	0.167	0.152	0.377
0.30	2.404	4.31	2.70	0.213	0.175	0.178	0.412
0.40	2.405	4.51	2.76	0.244	0.184	0.198	0.441
0.60	2.407	4.65	2.89	0.260	0.194	0.200	0.468
0.80	2.409	4.71	2.89	0.266	0.201	0.199	0.481
1.00	2.411	4.75	2.91	0.271	0.204	0.199	0.490
1.50	2.415	4.82	2.95	0.281	0.210	0.200	0.505
2.00	2.420	4.85	2.96	0.286	0.213	0.202	0.511
3.00	2.428	4.90	2.98	0.296	0.215	0.207	0.520
4.00	2.436	4.94	2.99	0.315	0.218	0.212	0.527
6.00	2.452	5.01	3.01	0.319	0.222	0.218	0.540
8.00	2.467	5.05	3.02	0.327	0.226	0.220	0.551
10.00	2.482	5.09	3.04	0.335	0.230	0.222	0.561

triaxial loading at 1 kbar confining pressure. The rock has been loaded and unloaded several times to determine in some detail its characteristic moduli at various shear-stress states, both on increasing and on decreasing pressure. At these confining pressures (similar to overburden) the rock shows no evidence of the dilation characteristic of the onset of large-scale fracturing. In contrast, in an atmospheric confining pressure test, the rock showed evidence of dilation at approximately 500 bar $\sigma_1 - \sigma_3$, and continued to dilate until it failed at 1.6 kbar. At 1 kbar confining pressure the rock shows an increase in volume only within several hundred bars of failure (~95% of failure stress). The initial loading moduli ($\sigma_1 - \sigma_3$ = 100 bar) from Figs. 7 and 8 are μ = 0.206 Mbar, ν = 0.13, and an effective K = 0.212 Mbar. With increasing axial load μ becomes 0.110 Mb and ν = 0.26 at 3.2 kbar $\sigma_1 - \sigma_3$; as Fig. 8 shows this trend is reversed on unloading. This latter feature presumably represents internal friction within the sample, which causes a hysteretic effect by preventing the immediate relaxation of deformation along cracks and fractures and around grain boundaries. Considering the nature of the rock, deformation by movement of individual grains probably accounts for most of the non-linearity shown in Fig. 7 and in all other triaxial tests on this material. The magnitude of this effect is noticeably dependent on confining pressure, which serves to reduce both curvature and hysteresis.

Upon initial loading at a confining pressure of 1 kbar, the siltstone from 8999 ft gave a μ = 0.157 Mbar, ν = 0.13, and an effective K = 0.181 Mbar. At $\sigma_1 - \sigma_3$ of 3.2 kbar the rock had deformed sufficiently to give μ = 0.096 Mbar and ν = 0.29,

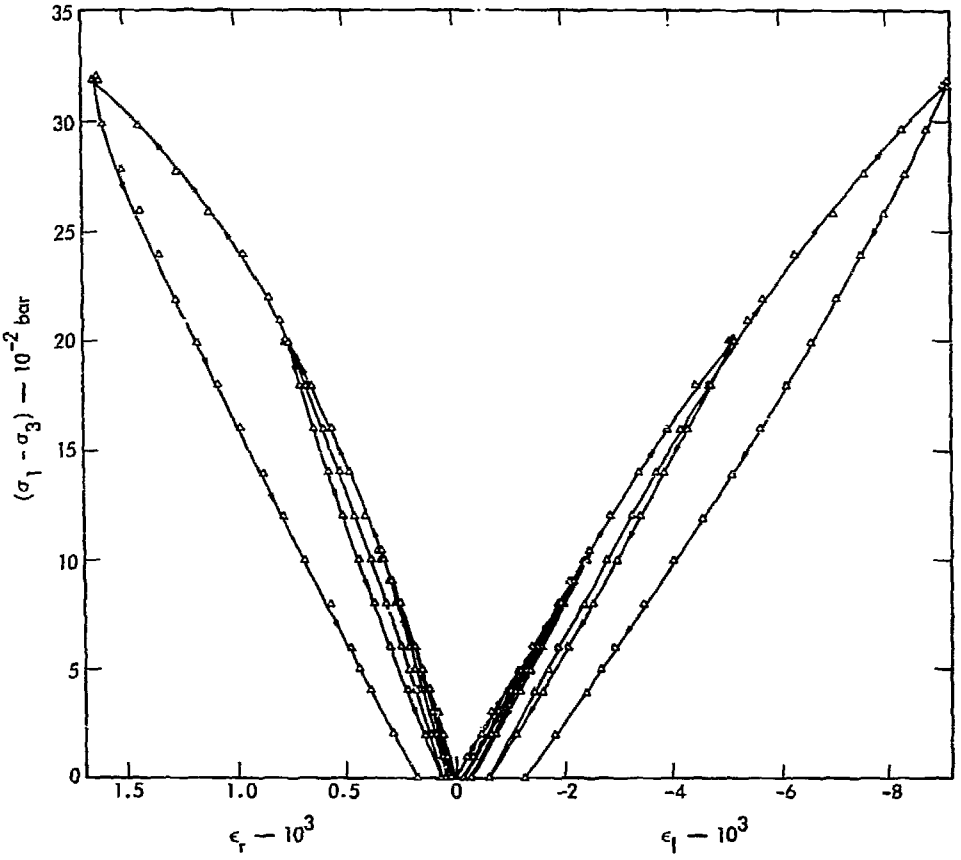

Fig. 7. 10,237 ft: Radial and longitudinal strain as a function of $\sigma_1 - \sigma_3$ at 1 kbar confining pressure.

with an effective K = 0.200 Mbar. The sandstone from the 8945-ft level is very nearly identical to the 10,237-ft material, although slightly more resistant to deformation: μ = 0.201 Mbar, ν = 0.12, and the effective K = 0.208 Mbar on initial loading at 1 bar confining pressure. This observation is in agreement with the previously mentioned results obtained for the two rocks on hydrostatic loading.

Figures 9 and 10 show the results of a one-dimensional strain ($\epsilon_r = 0$) loading experiment carried out from 1 kbar confining pressure on the sandstone from 10,237 ft. This experiment simulates stress-strain conditions during the passage of a plane shock wave front, although at strain-rates not even remotely comparable. It is noteworthy that this loading path does not appear to intersect the failure envelope, and in fact departs from it at high shear stress. The initial loading along this path yields values for the moduli of μ = 0.200 Mbar, ν = 0.14, and an

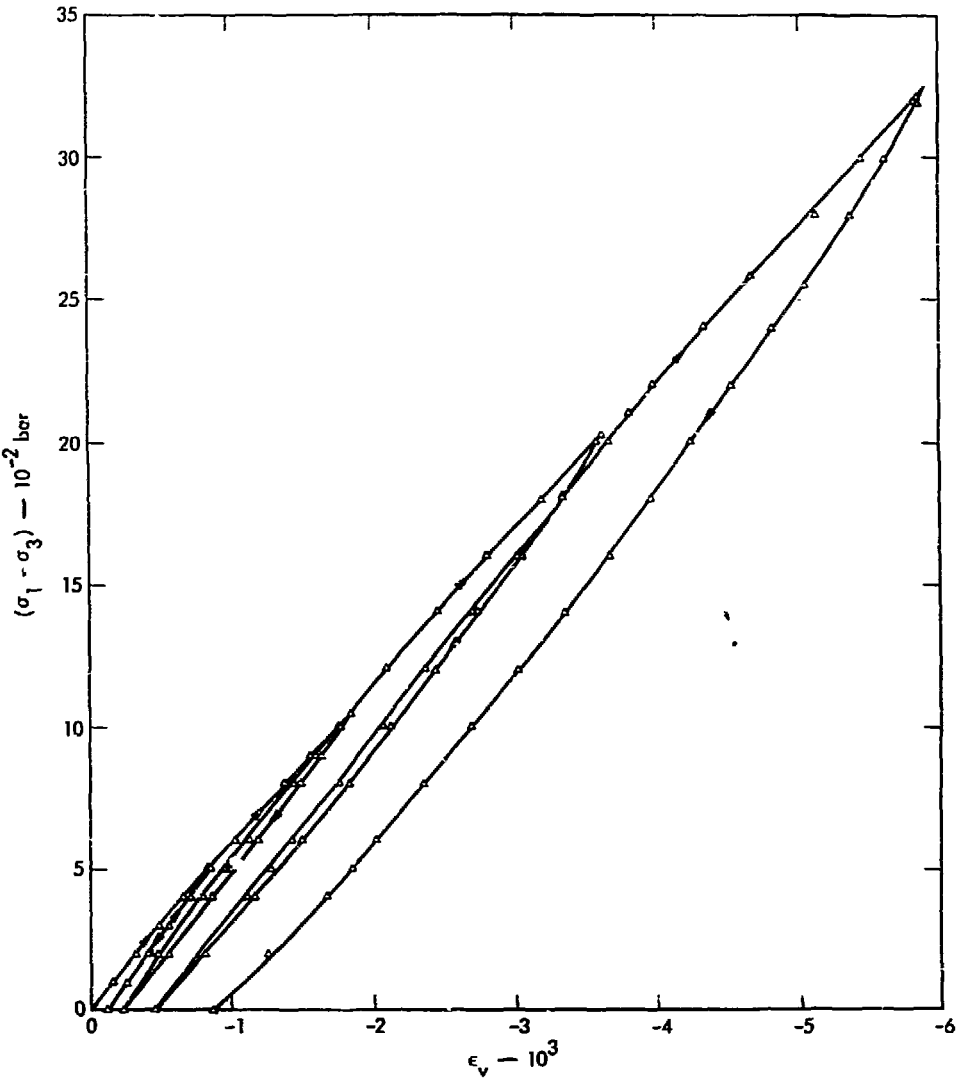

Fig. 8. 10,237 ft: Volume strain as a function of $\sigma_1 - \sigma_3$ at 1 kbar confining pressure.

effective K = 0.222 Mbar, in excellent agreement with initial values determined in triaxial loading. As the rock deforms the effective moduli change; at 4 kbar $\sigma_1 - \sigma_3$ μ = 0.145 Mbar and ν = 0.19; at 7 kbar end load pressure μ = 0.059 Mbar and ν = 0.31. The change in these values reflects the inelastic deformation of the rocks. Several unloading paths were considered and executed after the peak of the one-dimensional strain loading curve was reached. Figures 9 and 10 show the results

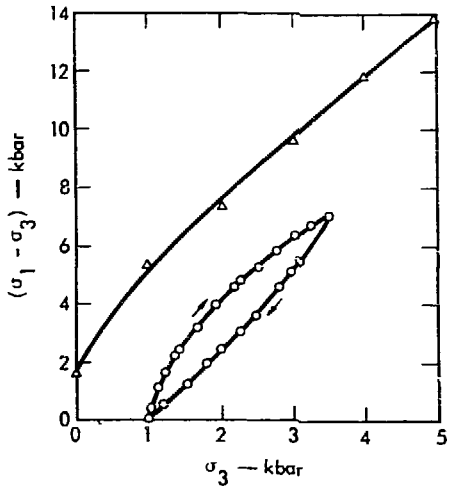

Fig. 9. 10,237 ft: $\sigma_1 - \sigma_3$ versus confining pressure with $\epsilon_r = 0$. The failure envelope from Fig. 1 is shown for comparison.

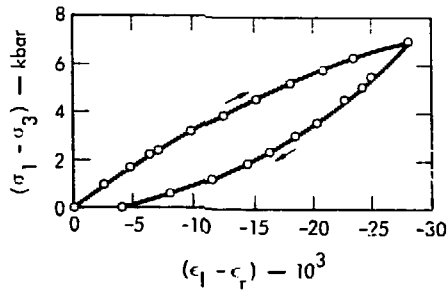

Fig. 10. 10,237 ft: Shear strain as a function of $\sigma_1 - \sigma_3$ from 1 kbar with $\epsilon_r = 0$.

obtained on one-dimensional unloading. The pronounced hysteresis is again representative of internal friction within the rock. In another test, as an extreme unloading path, it was assumed that partical velocity would remain constant behind the shock wave. This forces the unloading path in the direction of the failure surface. However, for this rock the path did not intersect the envelope, measured strains showed no marked evidence of instabilities, and the specimen was recovered intact.

In order to determine the effect of water on the loading moduli, a one-dimensional strain loading experiment was carried out on a 50%-saturated sample. No effect on loading moduli was observed, in agreement with the yield strength data.

The siltstone (8999 ft) showed initial loading moduli of $\mu = 0.154$ Mbar, $\nu = 0.12$ and an effective K = 0.178 Mbar. At 3 kbar $\sigma_1 - \sigma_3$ extensive inelastic deformation had taken place, and $\mu = 0.106$ Mbar, $\nu = 0.27$, and the effective K = 0.197 Mbar.

Conclusions

From the data obtained we believe that we have enough information to adequately characterize the media involved. Various stress-strain states yield concordant results. Thus, for instance, we may state with a high degree of confidence that the initial deformation moduli for the sandstone from 10,237 ft are $\mu = 0.200$ Mbar, $\nu = 0.13$, and K = 0.210 Mbar. Other sandstones (8945 ft and 11,060 ft) are similar in their deformational properties. These moduli change with stress, the change being dependent on the exact loading path and on the level of applied shear stress. With increasing shear stress, the shear modulus decreases and Poisson's ratio increases as the material deforms. Significantly, there appears to be little or no

purely elastic region under shear stress in any of the samples studied: the shear stress-shear strain plots show no linear behavior. This reflects the internal fabric of the rock composed of grains surrounded by a fine detrital matrix consisting largely of sheet-silicate minerals, allowing the grains to move quite easily relative to one another on the application of a small shear stress. Optical observations reveal that very little fracturing occurs in the samples from these tests.[1] The high percentage of quartz grains in the sandstones is reflected in the low initial value of Poisson's ratio. Specifically, this indicates a high value of the shear modulus relative to the bulk modulus and is characteristic of sandstones with high quartz content. Detrital quartz grains are usually less well rounded than any of the other common detrital materials and tend to form interlocking networks which present a relatively high initial resistance to shear stress. In pure quartzite sandstones this resistance is maintained at very high shear stress, but due to the nature of the matrix material we are considering, these sandstones very quickly begin to deform inelastically.

Triaxial compression tests on the sandstone from 10,237 ft show macroscopic brittle behavior at all confining pressures up to ~3 kbar. That is, the stress-longitudinal strain curve after the yield point showed sharp discontinuous changes in slope which could be visually correlated with through-going tensile- and shear-failure surfaces in the test sample. At confining pressures greater than ~4 kbar the material was ductile. Here, the stress-strain curves showed a monotonically decreasing slopes after the yield point, with various degrees of work hardening, depending upon pressure. Microscopic failure of the rock (at the highest pressures) was by homogeneously-distributed fracturing of the brittle quartz grains. Plastic flow occurred in the weaker matrix material. No through-going tensile or shear fracture or faulting was observed in this behavioral region.

The failure surfaces in shear stress-mean pressure space were constructed for the dry, 50%-saturated and fully-saturated sandstone. Both dry and 50%-saturated material yield failure surfaces which are nearly linear, with a transition from brittle to ductile behavior near 6 kbar mean pressure. The fully saturated material is very much weaker.

There is difficulty in getting the rock to fracture along one-dimensional loading paths, in triaxial tests at confining pressures greater than about 3 kbar, and upon unloading while still in compression. This would seem at first to indicate that fracturing would not be expected on a large scale as a result of a nuclear detonation. However, there are two factors which increase the probability of fracturing. First, under shock-loading, strain rates are much higher ($\sim 10^4$ sec^{-1}) and inelastic deformation is reduced, due mainly to inertial effects. This may result in loading closer to the failure surface. Second, upon unloading from any point on a one-dimensional loading path, one principal stress (either compressive or tensile) may become small, thus inducing unloading fractures in the material. Under shock loading, the quartz matrix of the sandstone may fail at mean pressures less than the calculated value of 30 kbar (based upon 50% fluid saturation and 8% porosity, as

noted above) due to intersection of the (postulated) steep Hugoniot loading path with the higher strain rate failure envelope. However, failure of the rock by shock loading is an unknown quantity at present, since no Hugoniot elastic limit has yet been determined for any Wagon Wheel sandstone.

Acknowledgments

E. M. Lilley, H. Louis, and H. R. Washington were instrumental in obtaining the data presented in this report. A. G. Duba contributed immeasurably to the interpretation and completion of the results. Discussions with I. Y. Borg were invaluable.

References

1. I. Y. Borg, private communication, July, 1970.
2. F. J. Pettijohn, Sedimentary Rocks, 2nd ed. (Harper and Bros., New York, 1957), p. 291.
3. P. D. Krynine, "The Megascopic Study and Field Classification of Sedimentary Rocks," J. Geol. 56, 130 (1948).
4. Leo Rogers, private communication, May, 1970.
5. D. R. Stephens and E. M. Lilley, "Loading-Unloading Pressure-Volume Curves for Rocks," Proc. ANS Topical Meeting, Engineering with Nuclear Explosives, Las Vegas, Nev., Jan. 14-16, 1970.
6. R. N. Schock, "Dynamic Elastic Moduli of Rocks under Pressure," Proc. ANS Topical Meeting, Engineering with Nuclear Explosives, Las Vegas, Nev., Jan. 14-16, 1970.
7. J. Handin and R. V. Hager, "Experimental Deformation of Sedimentary Rocks under Confining Pressure: Tests at Room Temperature on Dry Samples," Amer. Ass. Petrol. Geol. Bull. 41, 1 (1957).
8. H. C. Heard, "Transition from Brittle to Ductile Flow in Solenhofen Limestone as a Function of Temperature, Confining Pressure and Interstitial Fluid Pressure," in Rock Deformation, Memoir 79, Ed. by Griggs and Handin (Geological Society of America, Boulder, Colo., 1960), ch. 7, p. 193.
9. A. G. Duba and R. N. Schock, "Static Determination of the Deformational Properties of Solid Materials with Pressure," Lawrence Radiation Laboratory, Livermore, Rept. UCRL-50852 (1970).

Printed in USA. Available from the National Technical Information Center, National Bureau of Standards, U. S. Department of Commerce, Springfield, Virginia 22151
Price: Printed Copy $3.00; Microfiche $0.65.